RCEE

Research in Civil and Environmental Engineering

www.jrcee.com

Research in Civil and Environmental Engineering 1 (2013) 01-27

A free of parasitic shear strain formulation for plane element

Mohammad Rezaiee-Pajand [a*], Majid Yaghoobi[a]

[a] Department of Civil Engineering, Ferdowsi University of Mashhad, Mashhad, Iran

Keywords

Finite element

strain gradient

optimal element criteria

five-node rectangular element

plane elastic problem

A B S T R A C T

Two five-node rectangular elements are developed for analyzing two dimensional infinitesimal elastic strain problems. Several optimization criteria are elaborated, based on strain gradient notation. By utilizing these criteria and satisfying the equilibrium conditions, the SSDD and SSDI elements are formulated. Two additional five-node rectangular elements are also developed by using the traditional displacement approach. The robustness and accuracy of these four elements are assessed via numerical examples. The findings of the paper demonstrate the advantage of the SSDD and SSDI elements over the others. Moreover, these elements are free of the parasitic shear error.

1 Introduction

In the displacement formulation of finite elements, the effectiveness of elements is increased by increasing the degrees of freedom and/or by using equations of the higher degree for the interpolation functions. Increasing the number of degrees of freedom heightens to the complexity of the elements, which as a result, leads to additional computational cost. The years between 1965 and 1975, extensive effort was made to increase the accuracy of finite element analysis by constructing complex elements. As a result, many elements with different properties were introduced during these years. One of the greatest advances on simple and effective elements was developed during the mid 60's with the introduction of nonconforming elements. The patch test was also suggested during the same years to evaluate the adequacy of these elements. The reduced and selective integration methods were formulated in the following years and had a significant influence on the elimination of the modeling errors and producing efficient elements. The development of multi-field formulations was also a growing interest amongst

*Corresponding author (e-mail: *mrpajand@yahoo.com*).

researchers during those years, which led to the introduction of the hybrid and mixed formulations (Ghali and Chieslar, 1986; Pian, 1995).

More advanced formulations were originated by researchers during the 80's, which the free formulation (Bergan and Nygard, 1984) and assumed–strain formulation (MacNeal, 1978) were the most significant among them. These formulation strategies became the basis of creating more enhanced elements in the following years. It should be mentioned here that by using these elements, even coarse meshes produced reasonable results for practical applications. The advantages of these elements can be summarized as: simplicity, convergence, rotational invariance, rank sufficiency, equal accuracy for displacement and stress values, distortion insensitivity, mix ability with other elements, etc (Felippa, 2000).

While Bergan and Nygard (1984)were seeking to organize the free formulation method, Dow was making an attempt to develop another formulation, later known as the strain gradient notation (Dow, 1999). His motivation towards developing such a method was to investigate the errors which appeared in the finite element method and to eliminate these errors from the formulation. The founders of this notation effectively utilized the strain gradients to diagnose the error of finite elements. They managed to eliminate most of the deficiencies and errors of different elements in their formulation process by using the strain gradients.

During the early 90's, the Parameterized variational principle dramatically changed the knowledge towards highly efficient element formulations. Based on this principle, researchers managed to define a continuous space of the elastic functional. Different points in this space are the functional which if become stationary will lead to different formulations of the finite element method. Well known formulations, such as: potential energy, Hellinger-Reissner, and Hu-Washizu are the special points in this space. Making stationary of the continuous space of the functional, produces free parameters for the formulation of the element. As a result, this will lead to finite element templates (Felippa and Militello, 1990). Further investigations provided the fact that template based formulations are governed by a specific and similar algebraic structure, whereby attaining these formulations does not necessarily require to make the parameterized functional stationary. Assigning values to the free parameters of these templates will result in various types of the elements. Researchers' pursuit towards finding the most capable element for analyzing a structure led to the process of the optimizing finite element templates. This optimization consists of a step by step specialization procedure whereby the number of free parameters is reduced until an optimal element is attained. During this procedure, the analyst takes into account the effective properties of the element in each step. These properties will establish specific relations between the free parameters of the finite element template. The process of specialization, which is carried out via relevant tests on the templates, reduces the number of the independent free parameters. Moreover, it creates a group of the elements, which have similar properties. For example, all the elements of a group might have rotational invariance and/or they are all distortions insensitive. The step by step process of the specializing in the template continues until the optimal element is attained (Felippa, 2000).

The process of optimizing finite element templates is quite complicated and requires innovation. The large number of the free parameters, symbolic processing, and optimizing the entries of the matrix are the difficulties which are encountered in the process. Strain gradient notation is a comprehensible and simple interpretation which can be used in the free formulation process. For a displacement based formulation,

this notation reproduces the displacement interpolation field in terms of the strain states and therefore determines the origin of many errors, which arise in the finite element formulation.

This paper investigates new formulations, which are based on reasonable strain states. Displacement and strain interpolation fields can be obtained by equating other strain states to zero, in the global displacement and strain interpolation fields. It should be mentioned that the global displacement and strain interpolation fields contain all strain states. Different optimization criteria are also defined based on the strain states in this study. Taking advantage of these criteria and the equilibrium conditions, two five-node rectangular elements are attained for analyzing the plane-strain and plane-stress problems. The suggested formulation can easily separate the rigid body motions from the strain deformations. This advantage of the presented tactic makes it suitable for the co-rotational technique. In other words, the authors' strategy can be extended to include geometrical non-linear behavior.

The presented five-node rectangular elements are insensitive to the aspect ratio and have rotational invariance property. In the proposed formulation, the parasitic shear error can easily be eliminated by excluding the incorrect strain states from the shear strain polynomial. Good accuracy and rapid convergence to the exact solution are other merits of the suggested elements. By solving the benchmark structures, the efficiency of the authors' formulations will be shown. In addition, two other five-node rectangular elements are also developed based on the traditional displacement method, and they are utilized for the comparison study. In this article, the characteristics of all four elements are compared with each other and also with the other well known elements.

2 Strain gradient notation

In the common finite element formulation, the displacements are interpolated using a polynomial field function similar to the below form:

$$\begin{cases} u(x,y) = a_1 + a_2 x + a_3 y + a_4 x^2 + a_5 xy + a_6 y^2 + \dots \\ v(x,y) = b_1 + b_2 x + b_3 y + b_4 x^2 + b_5 xy + b_6 y^2 + \dots \end{cases} \quad (1)$$

It should be noted that the coefficients of these polynomial functions do not have any physical significance. Strain gradient notation translates these unfamiliar coefficients into strain states (Dow, 1999). For this purpose, a rectangular coordinate system is designated with its origin at an arbitrary position. Taylor's expansion of the strain field is then utilized about the origin. In a two-dimensional state, the strain field consists of three strain function as follows:

$$\begin{aligned} \varepsilon_x(x,y) &= (\varepsilon_x)_\circ + (\varepsilon_{x,x})_\circ x + (\varepsilon_{x,y})_\circ y + (\varepsilon_{x,xx})_\circ \left(\frac{x^2}{2}\right) + (\varepsilon_{x,xy})_\circ (xy) + (\varepsilon_{x,yy})_\circ \left(\frac{y^2}{2}\right) + \dots \\ \varepsilon_y(x,y) &= (\varepsilon_y)_\circ + (\varepsilon_{y,x})_\circ x + (\varepsilon_{y,y})_\circ y + (\varepsilon_{y,xx})_\circ \left(\frac{x^2}{2}\right) + (\varepsilon_{y,xy})_\circ (xy) + (\varepsilon_{y,yy})_\circ \left(\frac{y^2}{2}\right) + \dots \\ \gamma_{xy}(x,y) &= (\gamma_{xy})_\circ + (\gamma_{xy,x})_\circ x + (\gamma_{xy,y})_\circ y + (\gamma_{xy,xx})_\circ \left(\frac{x^2}{2}\right) + (\gamma_{xy,xy})_\circ (xy) + (\gamma_{xy,yy})_\circ \left(\frac{y^2}{2}\right) + \dots \end{aligned} \quad (2)$$

In these equations, the subscript ◦ specifies that the term regards the strain gradient value at the origin. These values are called strain states. The magnitude of the axial strain ε_x is denoted by $(\varepsilon_x)_\circ$, whereby $(\varepsilon_{x,x})_\circ$ and $(\varepsilon_{x,y})_\circ$ respectively represent the rate at which ε_x changes along the x and y axes in the neighborhood of the origin. Other coefficients are also determined by using this tactic. Following the mentioned process, the unfamiliar coefficients of the polynomial field function are replaced by the strain states. The strains are calculated by using the planar strain-displacement equations given in below:

$$\varepsilon_x = \frac{\partial u}{\partial x}\ , \quad \varepsilon_y = \frac{\partial v}{\partial y}\ , \quad \gamma_{xy} = \frac{\partial u}{\partial y} + \frac{\partial v}{\partial x} \tag{3}$$

It should be reminded that in the geometrically linear problems, the rigid body rotation defined in the following form:

$$r_r = \frac{1}{2}\left(\frac{\partial v}{\partial x} - \frac{\partial u}{\partial y}\right) \tag{4}$$

At the origin, strains and rotation will have the following values:

$$\begin{aligned} &(r_r)_\circ = (b_2 - a_3)/2 \\ &(\varepsilon_x)_\circ = a_2 \\ &(\varepsilon_y)_\circ = b_3 \\ &(\gamma_{xy})_\circ = a_3 + b_2 \end{aligned} \tag{5}$$

The rigid body rotation is equal to $(r_r)_\circ$. The unknown parameters are written in terms of strains as below:

$$\begin{aligned} &a_2 = (\varepsilon_x)_\circ \\ &a_3 = (\gamma_{xy}/2 - r_r)_\circ \\ &b_2 = (\gamma_{xy}/2 + r_r)_\circ \\ &b_3 = (\varepsilon_y)_\circ \end{aligned} \tag{6}$$

The coefficients of the quadratic terms of the field interpolation function can be determined by a similar approach. For this purpose, the following derivatives of the strains are utilized:

$$\begin{aligned} &\varepsilon_{x,x} = \frac{\partial \varepsilon_x}{\partial x} = \frac{\partial^2 u}{\partial x^2}, \qquad \varepsilon_{x,y} = \frac{\partial \varepsilon_x}{\partial y} = \frac{\partial^2 u}{\partial x \partial y} \\ &\varepsilon_{y,x} = \frac{\partial \varepsilon_y}{\partial x} = \frac{\partial^2 v}{\partial y \partial x}, \qquad \varepsilon_{y,y} = \frac{\partial \varepsilon_y}{\partial y} = \frac{\partial^2 v}{\partial y^2} \\ &\gamma_{xy,x} = \frac{\partial \gamma_{xy}}{\partial x} = \frac{\partial^2 u}{\partial y \partial x} + \frac{\partial^2 v}{\partial x^2}, \quad \gamma_{xy,y} = \frac{\partial \gamma_{xy}}{\partial y} = \frac{\partial^2 u}{\partial y^2} + \frac{\partial^2 v}{\partial x \partial y} \end{aligned} \tag{7}$$

By replacing the coordinates of the origin and solving the resulting set of equations, the coefficients of the displacement interpolation functions are determined as follows:

$$\begin{aligned} a_4 &= (\varepsilon_{x,x})_\circ/2, & b_4 &= (\gamma_{xy,x} - \varepsilon_{x,y})_\circ/2 \\ a_5 &= (\varepsilon_{x,y})_\circ, & b_5 &= (\varepsilon_{y,x})_\circ \\ a_6 &= (\gamma_{xy,y} - \varepsilon_{y,x})_\circ/2, & b_6 &= (\varepsilon_{y,y})_\circ/2 \end{aligned} \tag{8}$$

The remaining coefficients of the displacement interpolation field are obtained in a similar manner. Let $u_\circ$ and $v_\circ$ denote the rigid body translations along the x and y axes, the element's field functions can be written in the below form:

$$\begin{cases} u = u_\circ + (\varepsilon_x)_\circ x + (\gamma_{xy}/2 - r_r)_\circ y + (\varepsilon_{x,x})_\circ x^2/2 + (\varepsilon_{x,y})_\circ xy + (\gamma_{xy,y} - \varepsilon_{y,x})_\circ y^2/2 + \dots \\ v = v_\circ + (\gamma_{xy}/2 + r_r)_\circ x + (\varepsilon_y)_\circ y + (\gamma_{xy,x} - \varepsilon_{x,y})_\circ x^2/2 + (\varepsilon_{y,x})_\circ xy + (\varepsilon_{y,y})_\circ y^2/2 + \dots \end{cases} \tag{9}$$

The clear relation between strain states and the element's characteristics provides a comprehensible knowledge of its behavior. The result of this knowledge can be implemented for the error assessment, enhancement and increasing the capability of the element. In the proceeding text, the strain field function will be written in the following vector:

$$\begin{aligned} \varepsilon = \begin{Bmatrix} \varepsilon_x(x,y) \\ \varepsilon_y(x,y) \\ \gamma_{xy}(x,y) \end{Bmatrix} &= \begin{Bmatrix} (\varepsilon_x)_\circ \\ (\varepsilon_y)_\circ \\ (\gamma_{xy})_\circ \end{Bmatrix} + \begin{Bmatrix} (\varepsilon_{x,x})_\circ \\ (\varepsilon_{y,x})_\circ \\ (\gamma_{xy,x})_\circ \end{Bmatrix} x + \begin{Bmatrix} (\varepsilon_{x,y})_\circ \\ (\varepsilon_{y,y})_\circ \\ (\gamma_{xy,y})_\circ \end{Bmatrix} y + \\ &+ \begin{Bmatrix} (\varepsilon_{x,xx})_\circ \\ (\varepsilon_{y,xx})_\circ \\ (\gamma_{xy,xx})_\circ \end{Bmatrix} \left(\frac{x^2}{2}\right) + \begin{Bmatrix} (\varepsilon_{x,xy})_\circ \\ (\varepsilon_{y,xy})_\circ \\ (\gamma_{xy,xy})_\circ \end{Bmatrix} (xy) + \begin{Bmatrix} (\varepsilon_{x,yy})_\circ \\ (\varepsilon_{y,yy})_\circ \\ (\gamma_{xy,yy})_\circ \end{Bmatrix} \left(\frac{y^2}{2}\right) + \dots \end{aligned} \tag{10}$$

The strain field is a result of summing up multiple modes, each multiplied by a scaling factor. Each of the terms; 1, x, y, $x^2/2$, xy, $y^2/2$ etc. are modes of the strain field, whereby their influence in the strain functions is governed by their relevant strain states. Each strain state is a scalar, which indicates the scaling factor of a specific mode of the strain function. The finite element formulation can be based on a number of these strain states. Selecting the relevant strain states depends on the effective modes of the strain functions. By equating other strain states to zero in the displacement interpolation field (Eq. (9)), the regarding polynomial is obtained. The important feature of this process is that the degree of the polynomial chosen for the strain functions can vary depending on the requirements of the problem at hand. This feature gains great value in the cases where the shear strain is of the lower order than the axial strain.

3 Equilibrium equations

For a homogeneous elastic continuum in a plane-stress or plane-strain state, the equilibrium equations are written in the following form:

$$\begin{cases} \dfrac{\partial \sigma_x(x,y)}{\partial x} + \dfrac{\partial \tau_{xy}(x,y)}{\partial y} + F_x(x,y) = 0 \\ \dfrac{\partial \tau_{xy}(x,y)}{\partial x} + \dfrac{\partial \sigma_y(x,y)}{\partial y} + F_y(x,y) = 0 \end{cases} \tag{11}$$

where, the functions $F_x(x,y)$ and $F_y(x,y)$ are respectively the force field functions along the x and y directions in a rectangular coordinate system. It is worth reminding that in planar problems, the gradient of the force field, in the perpendicular direction (z) to the plane of the element, is equal to zero. The stress fields are defined in the rectangular coordinate system. Utilizing the stress-strain relations, Eq. (11) can be rewritten in terms of the strain fields. Considering Hooke's law for a homogeneous elastic condition, the following relations are valid for a plane problem:

$$\begin{aligned} \sigma_x &= 2G\,\varepsilon_x + \lambda(\varepsilon_x + \varepsilon_y) \\ \sigma_y &= 2G\,\varepsilon_y + \lambda(\varepsilon_x + \varepsilon_y) \\ \tau_{xy} &= G\,\gamma_{xy} \end{aligned} \tag{12}$$

In the above equation, λ will be equal to $E\nu/((1+\nu)(1-2\nu))$, and $E\nu/((1+\nu)(1-\nu))$ for the plane-strain and plane-stress cases, respectively. The shear modulus, Poisson's ratio and elastic modulus, are denoted by G, ν and E, correspondingly. Introducing Eq. (12) into Eq. (11) will result in the following equilibrium equations:

$$\begin{cases} (2G+\lambda)\,\varepsilon_{x,x}(x,y) + \lambda\,\varepsilon_{y,x}(x,y) + G\,\gamma_{xy,y}(x,y) + F_x(x,y) = 0 \\ \lambda\,\varepsilon_{x,y}(x,y) + (2G+\lambda)\,\varepsilon_{y,y}(x,y) + G\,\gamma_{xy,x}(x,y) + F_y(x,y) = 0 \end{cases} \tag{13}$$

4 An optimal model

In order to attain a suitable formulation, specific criteria must be considered. These criteria are considered in the proceeding text.

4.1 Patch test

In order to carry out the patch test, a number of elements are arbitrarily oriented with one or multiple shared nodes in between. In such a configuration, the inner node or nodes are surrounded by connected elements. The boundary nodes are then subjected to displacements and rotation that are consistent with the field of one of the strain states, for example, a constant strain field. The inner nodes have degrees of freedom in all directions and will translate according to the deformation of the patch. If the displacements of the inner nodes and the stress states of all points in the patch converge to their correct values as the size of the patch becomes infinitesimally small, the result is satisfactory.

It is obvious that if all the strain states of an actual known field are to be used in the assumed strain field of an element, that element would yield exact results. In other words, the errors which arise in the

formulation of the element are due to the fact that some actual strain states are not incorporated. The reasons behind the incapability of incorporating actual strain states are; (1) unawareness of strain states of an actual strain field and (2) avoiding complicated analyzes. An actual strain field in a constant state, generally consists of six strain states $u_\circ$, $v_\circ$, $(r)_\circ$, $(\varepsilon_x)_\circ$, $(\varepsilon_y)_\circ$ and $(\gamma_{xy})_\circ$. The constant patch test can be carried out with these states introduced into the assumed strain field of the element. Therefore, applying the six strain states mentioned above is a necessity for convergence.

4.2 In-plane pure bending test

Felippa used this test to find the optimal flexural template (Felippa, 2003a, b; Felippa, 2006). He discussed the response of the template to the in-plane bending along the x and y axes by evaluating the ratios of the energy. For this purpose, the Euler-Bernouli planar beam is utilized. In order to study the bending behavior of the beam, in the x direction, the beam of Fig. (1) is considered. This structure has a cross section equal to b×h, with a moment of M_x at the free ends.

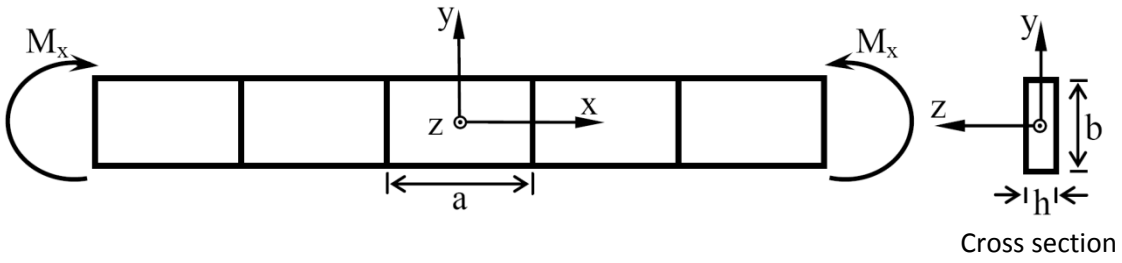

Fig. 1 In-plane pure bending test along the x axes

Ignoring the complicated behavior of the two ends, the majority of the beam will undergo a constant bending moment of $M(x)=M_x$, which will produce a stress field equal to $\sigma_x=-M_x y/I_b$. Noting that $I_b=hb^3/12$ and $\sigma_y=\tau_{xy}=0$. To study the structural behavior in the y direction, the beam of Fig. (2) is assumed. This structure is subject to M_y at the free ends. The bending moment along the beam is equal to $M(y)=M_y$, which results in a the stress field of $\sigma_y=M_y x/I_a$, with $I_a=ha^3/12$ and $\sigma_x=\tau_{xy}=0$. It should be reminded that these are exact results obtained from the elastic theory of the beams.

The internal elastic energy which is stored in the a×b section of this beam has the following value:

$$U_x^{beam}=\frac{6aM_x^{\,2}}{E\,b^3h}$$
$$U_y^{beam}=\frac{6bM_y^{\,2}}{E\,a^3h} \qquad (14)$$

In addition, the potential energy of the a×b section is also calculated when the beam is subjected to M_x and M_y. It is clear from Figures 1 and 2, the moments M_x and M_y will bend the structure in the xy plane. If this section is composed of only one rectangular element, the potential energy can be written in the following form:

$$U_x^{panel} = \frac{1}{2}\mathbf{D}_{bx}{}^T\mathbf{K}\mathbf{D}_{bx}$$
$$U_y^{panel} = \frac{1}{2}\mathbf{D}_{by}{}^T\mathbf{K}\mathbf{D}_{by} \qquad (15)$$

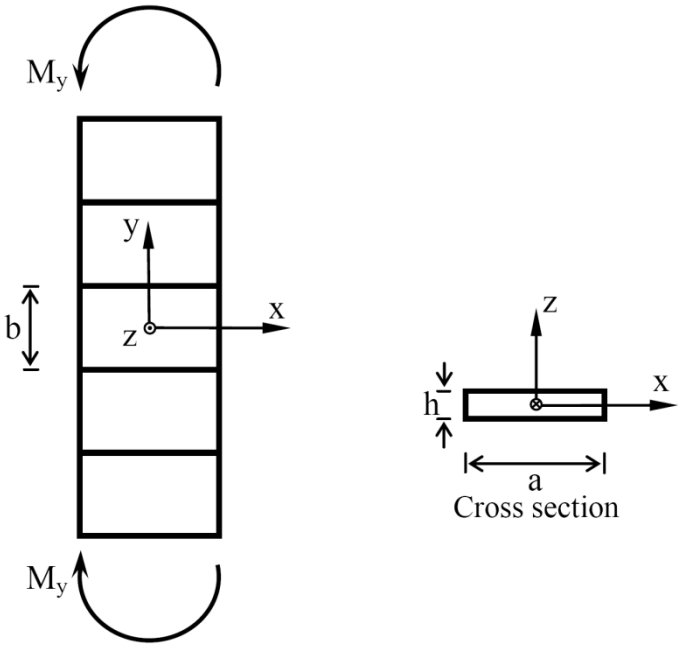

Fig. 2 In-plane pure bending test along the y axes.

where, $\mathbf{D}_{bx}$ and $\mathbf{D}_{by}$ are the nodal displacement vectors corresponding to relevant stress fields resulted from M_x and M_y moments, respectively. The stiffness matrix of the rectangular element is denoted by **K**. It should be mentioned that this test can also be used for triangular elements. In this case, the potential energy is equal to the sum of the potential energies stored in the two triangular elements which section a×b is composed of. The displacements $\mathbf{D}_{bx}$ and $\mathbf{D}_{by}$ are essential to evaluating this potential energy. For this purpose, stress fields are obtained for both cases of in-plane bending, which are shown in Figures 1 and 2. These stress functions are given in the following relations:

$$\sigma_x = -\frac{12M_x y}{b^3 h} \quad , \quad \sigma_y = 0 \quad , \quad \tau_{xy} = 0 \qquad (16)$$

$$\sigma_x = 0 \quad , \quad \sigma_y = \frac{12M_y x}{a^3 h} \quad , \quad \tau_{xy} = 0 \qquad (17)$$

With stresses functions at hand, the strain field can be attained. Afterwards, the displacement fields are obtained by integration. The flexural energy ratios for the x and y directions are calculated as follows:

$$r_x = \frac{U_x^{panel}}{U_x^{beam}}$$
$$r_y = \frac{U_y^{panel}}{U_y^{beam}} \qquad (18)$$

If r_x=1 or r_y=1, the element will be capable of correctly represent bending in the desired direction. If r_x>1 or r_x<1, the element is overstiff or overflexible in x bending, respectively. Likewise, this condition is similar to the y bending. In the case where r_x=1 or r_y=1, for any ratio of a/b, the element will be bending optimal. Finally, if a>>b results in r_x>>1 or if b>>a results in r_y>>1, shear locking will occur in the element. This test will now be investigated based on the strain states. If the beam is subjected to M_x, the actual stress field is as follows:

$$\sigma_x = \alpha_1 + \alpha_2 y \quad , \quad \sigma_y = 0 \quad , \quad \tau_{xy} = 0 \qquad (19)$$

The stress function, σ_x, has a linear variation along the y direction, and the coefficients α_1 and α_2 are constants. Base on Hooke's law, the strain field can be attained in the following form:

$$\varepsilon_x = \beta_1 + \beta_2 y \quad , \quad \varepsilon_y = \beta_3 + \beta_4 y \quad , \quad \gamma_{xy} = 0 \qquad (20)$$

where, $\beta_1 = \alpha_1 / E$, $\beta_2 = \alpha_2 / E$, $\beta_3 = -\nu\alpha_1 / E$ and $\beta_4 = -\nu\alpha_2 / E$. Poisson's ratio is denoted by ν and E represents the elastic modulus. Eq. (20) indicates that in the aforementioned actual strain field, only the strain states $u_\circ, v_\circ, (r_r)_\circ, (\varepsilon_x)_\circ, (\varepsilon_y)_\circ, (\varepsilon_{x,y})_\circ$ and $(\varepsilon_{y,y})_\circ$ will be present. In a similar manner, If the beam is subjected to M_y, the actual strain field will consist of $u_\circ, v_\circ, (r_r)_\circ, (\varepsilon_x)_\circ, (\varepsilon_y)_\circ, (\varepsilon_{x,x})_\circ$ and $(\varepsilon_{y,x})_\circ$. Therefore, in order to obtain the actual solution for an in-plane flexural problem, only the strain states $u_\circ$, $v_\circ, (r_r)_\circ, (\varepsilon_x)_\circ, (\varepsilon_y)_\circ, (\varepsilon_{x,x})_\circ, (\varepsilon_{x,y})_\circ, (\varepsilon_{y,x})_\circ$ and $(\varepsilon_{y,y})_\circ$ have to be taken into account. It should also be mentioned that the bending test, based on strain states, does not impose any limitations on the geometric shape of the element or the configuration of the mesh. In other words, this test not only can cover triangular and rectangular elements, but other elements as well.

4.3 Rotational invariance

In a number of the specific elements, properties of the element will not change with rotation of the coordinate system. These elements fall in the category of the rotational invariance elements. Since elements can be configured with different rotational orientation in the mesh of a structure, the element should be rotational invariance. Incomplete interpolation polynomials produce strain states that are not invariant with rotation. This lack of invariance means that the strains in elements based on incomplete polynomials can depend on the orientation of the element. Hence, rotational invariance is a result of the inclusion of all strain field terms with no algebraic order. For example, rotational mapping of a constant strain state is as follows:

$$
\begin{aligned}
(\varepsilon_{x'})_{\circ} &= (\varepsilon_{x})_{\circ}\cos^2\theta + (\varepsilon_{y})_{\circ}\sin^2\theta + (\gamma_{xy})_{\circ}\sin\theta\cos\theta \\
(\varepsilon_{y'})_{\circ} &= (\varepsilon_{x})_{\circ}\sin^2\theta + (\varepsilon_{y})_{\circ}\cos^2\theta - (\gamma_{xy})_{\circ}\sin\theta\cos\theta \\
(\gamma_{x'y'})_{\circ} &= 2\left((\varepsilon_{y})_{\circ} - (\varepsilon_{x})_{\circ}\right)\sin\theta\cos\theta + (\gamma_{xy})_{\circ}(\cos^2\theta - \sin^2\theta)
\end{aligned}
\tag{21}
$$

According to this equation, an element is capable of representing constant strains with respect to any system of the coordinates, only if its formulation takes into account all three cases of the constant strain states. It should be mentioned that invariance constraint has been used by researchers in the development of fine element templates(Felippa, 2000; Felippa and Militello, 1999).

4.4 Parasitic shear

Shear locking is characterized by sharp increases in the stiffness and condition number as the length /thickness ratio of the element increases. The error elimination process of the shear locking has been demonstrated by numerical example (Dow and Byrd, 1988). It should be added, this kind of error is caused by the inherent nature of the polynomials used and cannot be directly eliminated. Fortunately, its effects can be controlled by correcting the stiffness matrix with factors that depend on element geometry or by placing limitations on element geometry (Dow, 1999).

The appearance of axial strain states in the shear strain interpolation function causes the parasitic shear effect, which itself will lead to stiffen of the element (Dow, 1999). Some literatures have mistaken this form of the error with the shear locking phenomenon. The utilization of the strain gradient notation provides a clear distinction between these two phenomena. In order to gain knowledge about parasitic shear error, the formulation of the four-node rectangular element is examined. The interpolation functions of this element consist of an incomplete polynomial which contains neither x^2 nor y^2 terms. The strain gradient notation of these terms is as follows:

$$
\begin{cases}
u = u_{\circ} + (\varepsilon_{x})_{\circ}\,x + (\gamma_{xy}/2 - r_{r})_{\circ}\,y + (\varepsilon_{x,y})_{\circ}\,xy \\
v = v_{\circ} + (\gamma_{xy}/2 + r_{r})_{\circ}\,x + (\varepsilon_{y})_{\circ}\,y + (\varepsilon_{y,x})_{\circ}\,xy
\end{cases}
\tag{22}
$$

Based on the strain-deformation relations (Eq. (3)), the interpolation functions of the element can be written in the following form:

$$
\begin{cases}
\varepsilon_{x}(x,y) = (\varepsilon_{x})_{\circ} + (\varepsilon_{x,y})_{\circ}\,y \\
\varepsilon_{y}(x,y) = (\varepsilon_{y})_{\circ} + (\varepsilon_{y,x})_{\circ}\,x \\
\gamma_{xy}(x,y) = (\gamma_{xy})_{\circ} + (\varepsilon_{x,y})_{\circ}\,x + (\varepsilon_{y,x})_{\circ}\,y
\end{cases}
\tag{23}
$$

The advantages and the deficiencies of this model can be investigated through Taylor's expansion of this polynomial. By examining the shear strain series, it is noticed that the shear strains are independent of the axial strain. In the shear strain interpolation function, two strain states $(\varepsilon_{x,y})_{\circ}$ and $(\varepsilon_{y,x})_{\circ}$ improperly appear. Hence, if the element undergoes flexural deformations, the strain states will be nonzero and will incorrectly represent a portion of the shear strain.

For elements which are formulated using the strain gradient notation, the parasitic shear error can easily be eliminated by excluding the incorrect strain states from the shear strain polynomial. However, it is impossible to remove the shear locking effect by not including some terms of interpolation function. Although the root of parasitic shear error was unknown before presentation of the strain gradient notation scheme, some techniques like the reduced integration and the selective integration methods were suggested to eliminate the error. This was due to the fact that the incorrect parts of the potential strain energy were removed by using such integration tactics. However, it should also be added that using these strategies for some elements will remove the correct strain models as well. This will result in false zero energy states. The parasitic shear error decreases as the finer meshes are used. However, even coarser meshes can produce good results if elements are exempted from this error. It should be noted that utilizing complete interpolation functions will prevent the appearance of this error. Considering the abovementioned statements, the following strain states will be used for the model:

$$u_\circ, v_\circ, (r_r)_\circ, (\varepsilon_x)_\circ, (\varepsilon_y)_\circ, (\gamma_{xy})_\circ, (\varepsilon_{x,x})_\circ, (\varepsilon_{x,y})_\circ, (\varepsilon_{y,x})_\circ, (\varepsilon_{y,y})_\circ, (\gamma_{xy,x})_\circ, (\gamma_{xy,y})_\circ \tag{24}$$

5 Formulation of the five-node general model

Based on the strain states in Eq. (24), the five-node general model will be formulated in this section. Using the reasonable strain states, the displacement field of this model is defined as below:

$$\begin{cases} u = u_\circ + (\varepsilon_x)_\circ x + (\gamma_{xy}/2 - r_r)_\circ y + (\varepsilon_{x,x})_\circ x^2/2 + (\varepsilon_{x,y})_\circ xy + (\gamma_{xy,y} - \varepsilon_{y,x})_\circ y^2/2 \\ v = v_\circ + (\gamma_{xy}/2 + r_r)_\circ x + (\varepsilon_y)_\circ y + (\gamma_{xy,x} - \varepsilon_{x,y})_\circ x^2/2 + (\varepsilon_{y,x})_\circ xy + (\varepsilon_{y,y})_\circ y^2/2 \end{cases} \tag{25}$$

The strain field is obtained as follows:

$$\begin{cases} \varepsilon_x(x,y) = (\varepsilon_x)_\circ + (\varepsilon_{x,x})_\circ x + (\varepsilon_{x,y})_\circ y \\ \varepsilon_y(x,y) = (\varepsilon_y)_\circ + (\varepsilon_{y,x})_\circ x + (\varepsilon_{y,y})_\circ y \\ \gamma_{xy}(x,y) = (\gamma_{xy})_\circ + (\gamma_{xy,x})_\circ x + (\gamma_{xy,y})_\circ y \end{cases} \tag{26}$$

Eq. (13) is rewritten in the following form:

$$\begin{cases} \gamma_{xy,y}(x,y) = -\dfrac{(2G+\lambda)\,\varepsilon_{x,x}(x,y) + \lambda\,\varepsilon_{y,x}(x,y) + F_x(x,y)}{G} \\ \gamma_{xy,x}(x,y) = -\dfrac{\lambda\,\varepsilon_{x,y}(x,y) + (2G+\lambda)\,\varepsilon_{y,y}(x,y) + F_y(x,y)}{G} \end{cases} \tag{27}$$

Introducing the strain fields of Eq. (26) into Eq. (27) will result in the below values:

$$\begin{cases} (\gamma_{xy,y})_\circ = -\dfrac{(2G+\lambda)\,(\varepsilon_{x,x})_\circ + \lambda\,(\varepsilon_{y,x})_\circ + F_x(x,y)}{G} \\ (\gamma_{xy,x})_\circ = -\dfrac{\lambda\,(\varepsilon_{x,y})_\circ + (2G+\lambda)\,(\varepsilon_{y,y})_\circ + F_y(x,y)}{G} \end{cases} \tag{28}$$

Based on Eq. (28), the two strain states $(\gamma_{xy,x})_\circ$ and $(\gamma_{xy,y})_\circ$ can be derived as a function of the other strain states. Utilizing these relations, the unknowns of this new formulation will reduce to 10. From this point, the formulation will continue for the remaining 10 unknowns. By utilizing Eq. (25), the following interpolation field can be rewritten:

$$\begin{cases} u = u_\circ - (r_r)_\circ y + (\varepsilon_x)_\circ x + (\gamma_{xy})_\circ \dfrac{y}{2} + (\varepsilon_{x,x})_\circ \left(\dfrac{x^2}{2} - \dfrac{(2G+\lambda)\, y^2}{2G}\right) + (\varepsilon_{x,y})_\circ xy \\ -(\varepsilon_{y,x})_\circ \left(\dfrac{(G+\lambda)y^2}{2G}\right) - \dfrac{F_x(x,y)\, y^2}{2G} \\ v = v_\circ + (r_r)_\circ x + (\varepsilon_y)_\circ y + (\gamma_{xy})_\circ \dfrac{x}{2} + (\varepsilon_{y,y})_\circ \left(\dfrac{y^2}{2} - \dfrac{(2G+\lambda)\, x^2}{2G}\right) + (\varepsilon_{y,x})_\circ xy \\ -(\varepsilon_{x,y})_\circ \left(\dfrac{(G+\lambda)\, x^2}{2G}\right) - \dfrac{F_y(x,y)\, x^2}{2G} \end{cases} \tag{29}$$

On the other hand, the strain interpolation field (Eq. (26)) will take the following form:

$$\begin{cases} \varepsilon_x(x,y) = (\varepsilon_x)_\circ + (\varepsilon_{x,x})_\circ x + (\varepsilon_{x,y})_\circ y \\ \varepsilon_y(x,y) = (\varepsilon_y)_\circ + (\varepsilon_{y,x})_\circ x + (\varepsilon_{y,y})_\circ y \\ \gamma_{xy}(x,y) = (\gamma_{xy})_\circ - \dfrac{\lambda(\varepsilon_{x,y})_\circ + (2G+\lambda)(\varepsilon_{y,y})_\circ + F_y(x,y)}{G} x - \dfrac{(2G+\lambda)(\varepsilon_{x,x})_\circ + \lambda(\varepsilon_{y,x})_\circ + F_x(x,y)}{G} y \end{cases} \tag{30}$$

It is possible to define the strain states vector as below:

$$\hat{\mathbf{q}}^T = [u_\circ \quad v_\circ \quad (r_r)_\circ \quad (\varepsilon_x)_\circ \quad (\varepsilon_y)_\circ \quad (\gamma_{xy})_\circ \quad (\varepsilon_{x,x})_\circ \quad (\varepsilon_{y,x})_\circ \quad (\varepsilon_{x,y})_\circ \quad (\varepsilon_{y,y})_\circ] \tag{31}$$

According to this equation, the strain interpolation field is written in the below matrix form:

$$\boldsymbol{\varepsilon} = \hat{\mathbf{B}}_q . \hat{\mathbf{q}} + \tilde{\boldsymbol{\varepsilon}}$$

$$\hat{\mathbf{B}}_q = \begin{bmatrix} 0 & 0 & 0 & 1 & 0 & 0 & x & 0 & y & 0 \\ 0 & 0 & 0 & 0 & 1 & 0 & 0 & x & 0 & y \\ 0 & 0 & 0 & 0 & 0 & 1 & -\dfrac{(2G+\lambda)}{G} y & -\dfrac{\lambda}{G} y & -\dfrac{\lambda}{G} x & -\dfrac{(2G+\lambda)}{G} x \end{bmatrix} \tag{32}$$

$$\tilde{\boldsymbol{\varepsilon}} = \begin{bmatrix} 0 \\ 0 \\ -\dfrac{F_x(x,y)}{G} y - \dfrac{F_y(x,y)}{G} x \end{bmatrix} \tag{33}$$

In addition, the displacement interpolation field is obtained in matrix form as follows:

$$\mathbf{U}=\hat{\mathbf{N}}_{\mathbf{q}}.\hat{\mathbf{q}}+\tilde{\mathbf{U}} \tag{34}$$

$$\hat{\mathbf{N}}_{\mathbf{q}}=\begin{bmatrix} 1 & 0 & -y & x & 0 & \frac{y}{2} & \frac{x^2}{2}-\frac{(2G+\lambda)y^2}{2G} & -\frac{(G+\lambda)y^2}{2G} & xy & 0 \\ 0 & 1 & x & 0 & y & \frac{x}{2} & 0 & xy & -\frac{(G+\lambda)x^2}{2G} & \frac{y^2}{2}-\frac{(2G+\lambda)x^2}{2G} \end{bmatrix} \tag{35}$$

$$\tilde{\mathbf{U}}=\begin{bmatrix} -\frac{F_x(x,y)}{2G}y^2 \\ -\frac{F_y(x,y)}{2G}x^2 \end{bmatrix} \tag{36}$$

The assumed field can be implemented for any five-node element. Introducing the nodal coordinates into Eq. (34) will yield the nodal displacement vector as below:

$$\mathbf{D}=\hat{\mathbf{G}}_{\mathrm{q}}.\hat{\mathbf{q}}+\tilde{\mathbf{D}}=\hat{\mathbf{D}}+\tilde{\mathbf{D}} \tag{37}$$

The $\hat{\mathbf{G}}_{\mathrm{q}}$ matrix is obtained by placing the nodal coordinates into $\hat{\mathbf{N}}_{\mathrm{q}}$. It should be mentioned that $\hat{\mathbf{G}}_{\mathrm{q}}$ provides a relation between the strain state vector and the displacement vector. Therefore, the boundary conditions can be applied to the formulation as follows:

$$\hat{\mathbf{D}}=\hat{\mathbf{G}}_{\mathrm{q}}.\hat{\mathbf{q}} \quad , \quad \hat{\mathbf{q}}=\hat{\mathbf{G}}_{\mathrm{q}}^{-1}.\hat{\mathbf{D}} \tag{38}$$

Since the majority of the boundary conditions are in the form of displacements, the displacement and strain interpolation fields can be written in terms of the nodal displacement vector. Utilizing Eqs. (34) and (37), the following relations are obtained:

$$\mathbf{U}=\hat{\mathbf{N}}_{\mathrm{q}}.\hat{\mathbf{q}}+\tilde{\mathbf{U}}=\hat{\mathbf{N}}_{\mathrm{q}}.(\hat{\mathbf{G}}_{\mathrm{q}}^{-1}.\hat{\mathbf{D}})+\tilde{\mathbf{U}}=\hat{\mathbf{N}}.\hat{\mathbf{D}}+\tilde{\mathbf{U}} \tag{39}$$

$$\hat{\mathbf{N}}=\hat{\mathbf{N}}_{\mathrm{q}}.\hat{\mathbf{G}}_{\mathrm{q}}^{-1} \tag{40}$$

Eqs. (32) and (37) result in the below form:

$$\boldsymbol{\varepsilon}=\hat{\mathbf{B}}_{\mathrm{q}}.\hat{\mathbf{q}}+\tilde{\boldsymbol{\varepsilon}}=\hat{\mathbf{B}}_{\mathrm{q}}.(\hat{\mathbf{G}}_{\mathrm{q}}^{-1}.\hat{\mathbf{D}})+\tilde{\boldsymbol{\varepsilon}}=\hat{\mathbf{B}}.\hat{\mathbf{D}}+\tilde{\boldsymbol{\varepsilon}} \tag{41}$$

$$\hat{\mathbf{B}}=\hat{\mathbf{B}}_{\mathrm{q}}.\hat{\mathbf{G}}_{\mathrm{q}}^{-1} \tag{42}$$

On the other hand, the potential energy function is attained in terms of the elastic matrix (**E**) as follows:

$$\Pi=\frac{1}{2}\int\boldsymbol{\varepsilon}^{\mathrm{T}}.\mathbf{E}.\boldsymbol{\varepsilon}\,\mathrm{dv}-\int\mathbf{U}^{\mathrm{T}}.\mathbf{F}\,\mathrm{dv} \tag{43}$$

The displacement and strain interpolation fields (Eqs. (38) and (40)) are placed into the potential energy function. For this purpose, $\boldsymbol{\varepsilon}^{\mathbf{T}}.\mathbf{E}.\boldsymbol{\varepsilon}$ and $\mathbf{U}^{\mathbf{T}}.\mathbf{F}$ are calculated as below:

$$\boldsymbol{\varepsilon}^{\mathrm{T}}.\mathbf{E}.\boldsymbol{\varepsilon}=(\hat{\mathbf{D}}^{\mathrm{T}}.\hat{\mathbf{B}}^{\mathrm{T}}+\tilde{\boldsymbol{\varepsilon}}^{\mathrm{T}}).\mathbf{E}.(\hat{\mathbf{B}}.\hat{\mathbf{D}}+\tilde{\boldsymbol{\varepsilon}})=\hat{\mathbf{D}}^{\mathrm{T}}.\hat{\mathbf{B}}^{\mathrm{T}}.\mathbf{E}.\hat{\mathbf{B}}.\hat{\mathbf{D}}+\hat{\mathbf{D}}^{\mathrm{T}}.\hat{\mathbf{B}}^{\mathrm{T}}.\mathbf{E}.\tilde{\boldsymbol{\varepsilon}}+\tilde{\boldsymbol{\varepsilon}}^{\mathrm{T}}.\mathbf{E}.\hat{\mathbf{B}}.\hat{\mathbf{D}}+\tilde{\boldsymbol{\varepsilon}}^{\mathrm{T}}.\mathbf{E}.\tilde{\boldsymbol{\varepsilon}}$$

$$\mathbf{U}^{\mathrm{T}}.\mathbf{F}=(\hat{\mathbf{D}}^{\mathrm{T}}.\hat{\mathbf{N}}^{\mathrm{T}}+\tilde{\mathbf{U}}).\mathbf{F} \tag{44}$$

At this stage, the potential energy must be minimized. Introducing Eq. (43) into the potential energy function and differentiate with respect to the nodal displacements, the following relation is obtained:

$$\frac{\partial\Pi}{\partial\hat{\mathbf{D}}}=0$$
$$(\int\hat{\mathbf{B}}^{\mathrm{T}}.\mathbf{E}.\hat{\mathbf{B}}\,\mathrm{dv}).\hat{\mathbf{D}}+(0.5)\times\int\hat{\mathbf{B}}^{\mathrm{T}}.\mathbf{E}.\tilde{\boldsymbol{\varepsilon}}\,\mathrm{dv}+(0.5)\times\int\hat{\mathbf{B}}^{\mathrm{T}}.\mathbf{E}^{\mathrm{T}}.\tilde{\boldsymbol{\varepsilon}}\,\mathrm{dv}-\int\hat{\mathbf{N}}^{\mathrm{T}}.\mathbf{F}\,\mathrm{dv}=0 \tag{45}$$

This relation can be written in the below general form:

$$(\int\hat{\mathbf{B}}^{\mathrm{T}}.\mathbf{E}.\hat{\mathbf{B}}\,\mathrm{dv}).\hat{\mathbf{D}}=\int\hat{\mathbf{N}}^{\mathrm{T}}.\mathbf{F}\,\mathrm{dv}-(0.5)\times\int\hat{\mathbf{B}}^{\mathrm{T}}.\mathbf{E}.\tilde{\boldsymbol{\varepsilon}}\,\mathrm{dv}-(0.5)\times\int\hat{\mathbf{B}}^{\mathrm{T}}.\mathbf{E}^{\mathrm{T}}.\tilde{\boldsymbol{\varepsilon}}\,\mathrm{dv} \tag{46}$$

The stiffness matrix **K** is also obtained as follows:

$$\mathbf{K}=\int\hat{\mathbf{B}}^{\mathrm{T}}.\mathbf{E}.\hat{\mathbf{B}}\,\mathrm{dv} \tag{47}$$

Due to the symmetry of the stiffness matrix, the nodal load vector **P** is obtained as below:

$$\mathbf{P}=\int(\hat{\mathbf{N}}^{\mathrm{T}}.\mathbf{F}-(0.5)\times\hat{\mathbf{B}}^{\mathrm{T}}.\mathbf{E}.\tilde{\boldsymbol{\varepsilon}}-(0.5)\times\hat{\mathbf{B}}^{\mathrm{T}}.\mathbf{E}^{\mathrm{T}}.\tilde{\boldsymbol{\varepsilon}})\mathrm{dv}$$
$$\mathbf{P}=\int(\hat{\mathbf{N}}^{\mathrm{T}}.\mathbf{F}-\hat{\mathbf{B}}^{\mathrm{T}}.\mathbf{E}.\tilde{\boldsymbol{\varepsilon}})\mathrm{dv} \tag{48}$$

In order to find the load interpolation matrix, vector $\tilde{\boldsymbol{\varepsilon}}$ must be written in terms of the loading field. This is accomplished as below:

$$\tilde{\boldsymbol{\varepsilon}}=\begin{bmatrix} 0 \\ 0 \\ -\frac{F_x(x,y)}{G}y-\frac{F_y(x,y)}{G}x \end{bmatrix}=\begin{bmatrix} 0 & 0 \\ 0 & 0 \\ -\frac{y}{G} & -\frac{x}{G} \end{bmatrix}\begin{bmatrix} F_x(x,y) \\ F_y(x,y) \end{bmatrix}=\begin{bmatrix} 0 & 0 \\ 0 & 0 \\ -\frac{y}{G} & -\frac{x}{G} \end{bmatrix}\mathbf{F} \tag{49}$$

Placing Eq. (48) into Eq. (47) will result in the following relation:

$$\mathbf{P}=\int(\hat{\mathbf{N}}^{T}.\mathbf{F}-\hat{\mathbf{B}}^{T}.\mathbf{E}.\tilde{\boldsymbol{\varepsilon}})dv=\int(\hat{\mathbf{N}}^{T}.\mathbf{F}-\hat{\mathbf{B}}^{T}.\mathbf{E}.\begin{bmatrix} 0 & 0 \\ 0 & 0 \\ -\frac{y}{G} & -\frac{x}{G} \end{bmatrix}.\mathbf{F})dv=\int\hat{\mathbf{N}}_{F}{}^{T}.\mathbf{F}\,dv \tag{50}$$

As a result, the load interpolation matrix $\hat{\mathbf{N}}_F$ is obtained in the following form:

$$\hat{\mathbf{N}}_{F}{}^{T}=\hat{\mathbf{N}}^{T}-\hat{\mathbf{B}}^{T}.\mathbf{E}.\begin{bmatrix} 0 & 0 \\ 0 & 0 \\ -\frac{y}{G} & -\frac{x}{G} \end{bmatrix}$$

$$\hat{\mathbf{N}}_{F}=\hat{\mathbf{N}}-\begin{bmatrix} 0 & 0 & -\frac{y}{G} \\ 0 & 0 & -\frac{x}{G} \end{bmatrix}.\mathbf{E}.\hat{\mathbf{B}} \tag{51}$$

6 Creation of two special elements

The effectiveness of the five-node general formulation is verified through the creation of two special elements. For this purpose, the aforementioned model will be applied to a rectangular five-node element. For SSDD element, the placement of the nodes is similar to Fig. 3-1. The Fig. 3-1 shows a suitable arrangement of elements for the transition region, for instance, from side with three nodes to another one with two nodes. On the other hand, the element of Fig. 3-2 is useful for the homogeneous domain, with all sides having two nodes. The element of Fig. 3-1 has higher order of the compatibility condition in comparison to the element in Fig. 3-2.

SSDD is a direction-dependent element, but its geometry has a better form for compatibility. Figures 4-2 and 7-2 demonstrate suitable meshing for SSDD elements. The authors proposed another five-node element, which has one node in the center of element area. This new element is called SSDI, and it is shown in Figure 3-2. The condensation tactic can change it to the four-node element.

It should be mentioned that two other element labeled by CTE1 and CTE2 are also developed in this paper. These rectangular elements are utilized for comparison according to the traditional displacement formulation. The geometry of the CTE1 element is shown in Fig. 3-2. For this element, the displacement field is assumed to have below functions:

$$\begin{cases} u(x,y) = a_1 + a_2 x + a_3 y + a_4 xy + a_5 (x^2 + y^2) \\ v(x,y) = b_1 + b_2 x + b_3 y + b_4 xy + b_5 (x^2 + y^2) \end{cases} \quad (52)$$

On the other hand, Fig. 3-1 shows the geometry of the CTE2 element. For this element, the assumed displacement field is as follows:

$$\begin{cases} u(x,y) = a_1 + a_2 x + a_3 y + a_4 xy + a_5 x^2 \\ v(x,y) = b_1 + b_2 x + b_3 y + b_4 xy + b_5 x^2 \end{cases} \quad (53)$$

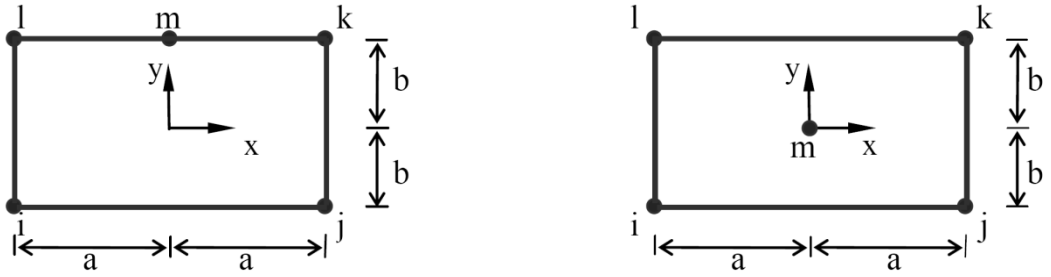

Fig. 3 The two geometric arrangements for the five-node elements

7 Numerical studies

In order to gain insight into the effectiveness of the proposed five-node rectangular elements, several benchmark problems, which are introduced by other researchers, are solved. The efficiency of the SSDD and SSDI elements in comparison to the CTE1 and CTE2 elements is evaluated via these plane problems. These structures have formerly been used by the other researchers for testing a variety of different elements, and their results are available (Eom *et al.*, 2009; Felippa, 2003a, b; Felippa and Alexander, 1992; Paknahad *et al.*, 2007). The mentioned elements are listed below:

1. StrainRP : 5-strain-mode element)Felippa, 2003b(
2. StressRP : 5-stress-mode element)Felippa, 2003b(
3. DispRP : Bilinear iso-P element)Felippa, 2003b(
4. BODT : a 3-node membrane element with drilling freedoms)Alvin *et al.*, 1992; Felippa, 2003a, b; Felippa and Alexander, 1992; Felippa and Militello, 1992(
5. Allman : Allman's element with spurious mode control(Allman, 1984; Eom et al., 2009)
6. ALL-EX : Allman 88 element, exactly integrated (Allman, 1988; Felippa, 2003b)
7. ALL-3i : Allman 88 element integrated by 3-point interior rule (Allman, 1988; Felippa, 2003a)
8. ALL-3m : Allman 88 element integrated by 3-midpoint rule (Allman, 1988; Felippa, 2003a)
9. ALL-LS : Allman 88 element, least-square strain fit (Allman, 1988; Felippa, 2003a)
10. ALL-7i : Allman 88 element integrated by the 7-internal-point rule (Allman, 1988; Felippa and Alexander, 1992)
11. CST : Constant strain triangle CST-3/6C(Felippa, 2003b)

12. FF84 : 1984 Free Formulation element of Bergan and Felippa (Bergan and Felippa, 1985; Felippa, 2003a)
13. LST-Ret : Retrofitted LST with (α_b=4/3) (Felippa, 2003a)
14. OPT : Optimally fabricated assumed natural deviatoric strain triangle (Felippa, 2003a)
15. EFF-AND : Designates indistinctly the optimal EFF or ANDES triangles (Felippa and Alexander, 1992)
16. FF : FF element with (β = ½) (Bergan and Felippa, 1985; Felippa and Alexander, 1992)
17. MEAS : The modified enhanced assumed strain triangle (Eom *et al.*, 2009; Yeo and Lee, 1996)
18. CSTHybrid : Cook's plane hybrid triangle (Cook, 1987; Eom *et al.*, 2009)
19. M3 : The macro element without tuning higher order stiffness parameter (Eom *et al.*, 2009)
20. SM3 : The macro element with tuned higher order stiffness parameter (Eom *et al.*, 2009)
21. OPT1 : Optimally fabricated assumed natural deviatoric strain triangle with alternative
22. formulation for higher order stiffness matrix (Paknahad *et al.*, 2007)
23. HW12-S, HW14-S, HW10-N, HW14-N, HW18: Mixed four-node elements based on the HuWashizu functional (Wisniewski and Turska, 2009)
24. HR5-S: HR element with five modes in skew coordinates (Wisniewski and Turska, 2006, 2009)
25. EADG4: Enhanced assumed displacement gradient element with four modes (Wisniewski and Turska, 2008, 2009)

7.1 Short cantilever beam under shear force at the free end

The first example is a short homogeneous cantilever beam, which is subjected to a parabolic shear force at its free end. In order to model the fixity at the other end of the beam, the nodal displacements on that side are set to zero. The exact deflection of the free end is equal to 0.35601 (Felippa, 2003a). As illustrated in Fig. 4-1, the beam has a length of 48, height of 12 and width of 1. The elastic modulus is equal to 30000 and the Poisson's ratio is 0.25. All values of this example are dimensionless. The total shear load acting on the beam is equal to 40.

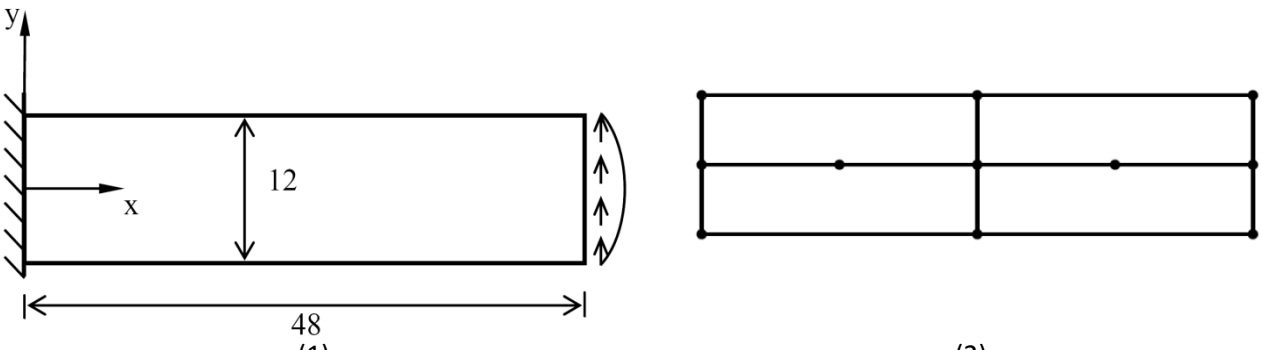

Fig. 4 Short cantilever beam under shear force.

The structure is modeled by the four five-node elements, SSDD, SSDI, CTE1 and CTE2, using the mesh subdivisions of Fig. 5, with N_y=2 and N_x=2,4,8,16,32, and also the mesh subdivisions of Fig.6, with N_y=4 and N_x=2,4,8,16,32, whereby; Nx represents the number of the elements along x, and N_y is the number of the elements along y. SSDD and CTE2 are direction-dependent elements, but their geometry had a better form for compatibility. Figure 4-2 demonstrates suitable meshing for SSDD and CTE2 elements.

These models are then compared with each other. In addition, the result of using the SSDD, SSDI, CTE1 and CTE2 elements and the results obtained by utilizing other elements are given in Table 1. The effectiveness of the SSDD and SSDI elements over other elements is then examined using this table. It is worth reminding; the exact solution of this problem is equal to 0.35601.

Figs. 5 and 6 indicate that by using the CTE2 element, the stiffness decreases as the numbers of elements increase. This property is clearly evident by comparison of the N_y=4 and N_y=2 cases. The SSDD, SSDI and CTE1 elements demonstrate insensitivity to the dimensions of the element and yield a uniform convergence towards the exact answer. The CTE1 element produces less error, for the case of N_y=4 than N_y=2, whereby the decrease in error becomes much more significant when coarser meshes are used. For a coarse mesh, the SSDD and SSDI elements are much efficient than the CTE1 element. In other words, they have a much smaller error. This difference in error decreases as finer meshes are used and the results converge to the exact solution. Comparing the results obtained by using SSDD, SSDI and other elements in Table 1 indicates that the SSDD and SSDI elements are almost the best in any mesh. Having a small error in the analysis of coarse meshes with a large aspect ratio, clearly demonstrates that the suggested elements are free from shear-locking.

Table 1 Exact deflection percentage of the short cantilever beam under end shear

Element	$N_x \times N_y$					
	2×2	**4×2**	**8×2**	**4×4**	**8×4**	**16×4**
strainRP	90.47	95.67	97.24	97.03	98.67	99.19
stressRP	91.94	97.22	98.80	97.41	99.08	99.59
DispRP	37.84	69.88	88.83	70.57	90.05	96.83
BODT	92.24	96.68	101.68	96.99	98.44	100.30
Allman	52.22	83.02	91.74	66.58	94.62	97.58
ALL-EX	26.16	70.71	89.43	56.93	89.63	96.88
ALL-3I	42.53	82.27	96.41	72.66	93.22	98.59
ALL-3M	12.39	54.23	82.70	31.81	81.84	94.78
ALL-LS	23.02	69.97	89.72	52.37	89.30	96.94
ALL-7I	26.16	70.71	89.43	56.93	89.63	96.88
CST	17.83	37.85	55.09	43.84	69.86	82.59
FF84	89.26	94.27	99.15	96.37	97.85	99.71
LST-Ret	56.71	79.58	70.86	83.79	93.53	91.10
OPT	92.24	96.68	101.68	96.99	98.44	100.30
FF	89.26	94.27	99.15	96.37	97.85	99.71
MEAS	17.93	38.01	55.18	43.90	69.90	82.60
CSTHybrid	74.30	92.38	100.79	91.44	97.49	99.96
M3	92.91	98.39	103.37	96.83	98.97	100.58
SM3	92.71	99.13	105.18	97.09	99.26	101.00
SSDD	92.77	97.61	98.96	97.94	99.32	99.73
CTE1	81.97	89.52	95.04	94.53	96.96	98.60
CTE2	95.98	101.47	103.09	102.93	104.66	105.21
SSDI	91.92	97.21	98.80	97.45	99.08	99.60

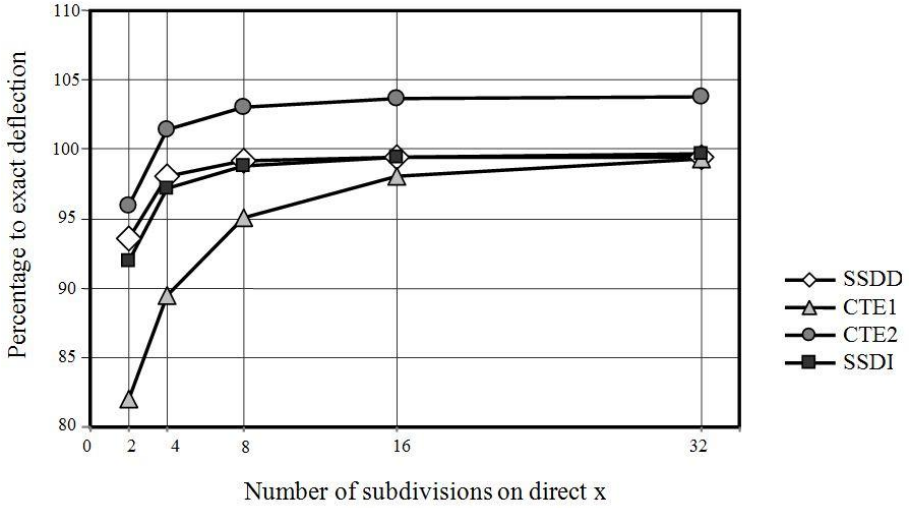

Figure 5.Deflection at the free end of the short cantilever beam for N_y=2

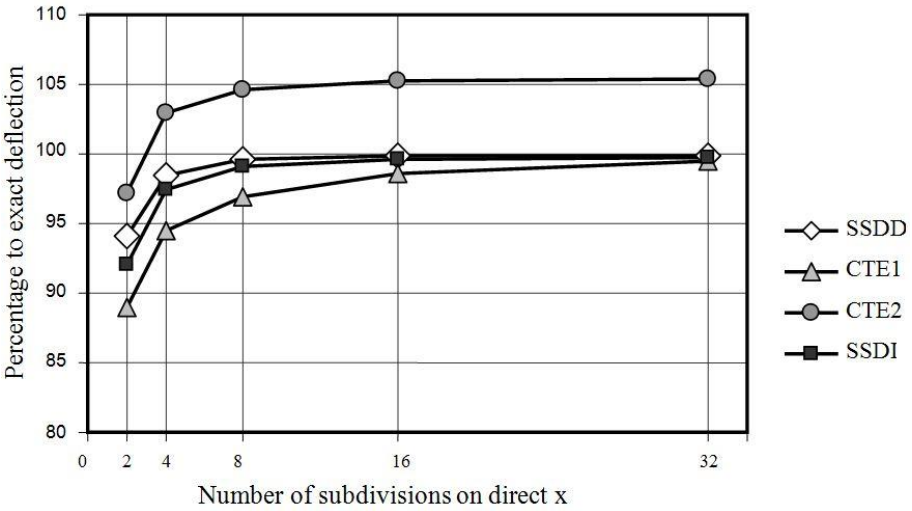

Figure 6.Deflection at the free end of the short cantilever beam for N_y=4

7.2 Slender cantilever beam under two different loads

The second benchmark problem is a homogeneous slender cantilever beam. This structure will once be subjected to a bending moment and once to a distributed parabolic shear at the free end. The nodes at the fixed end will have zero displacements. Based on the beam theory, the deflection of the free end of a beam with length L, moment of inertia Iz and elastic modulus E, under a bending moment M will be equal to ML2/(2EIz). The deflection of this beam under a shear force is Equal to PL3/(3EIz)+PL/(GAs). In these equations, As=5A/6 and Iz=hb3/12. The elastic modulus E and the shear modulus G are set to 7680 and 3072, respectively. As illustrated in Fig. 7-1, The length of the beam is 32, the height is 2 and the width is equal to h=1. The bending moment and the shear force applied to this beam are equal to M=1000 and P=46.7381, respectively. In both cases, the exact deflection of the beam's free end is equal to 100. Figure 7-2 demonstrates suitable meshing for SSDD and CTE2 elements.

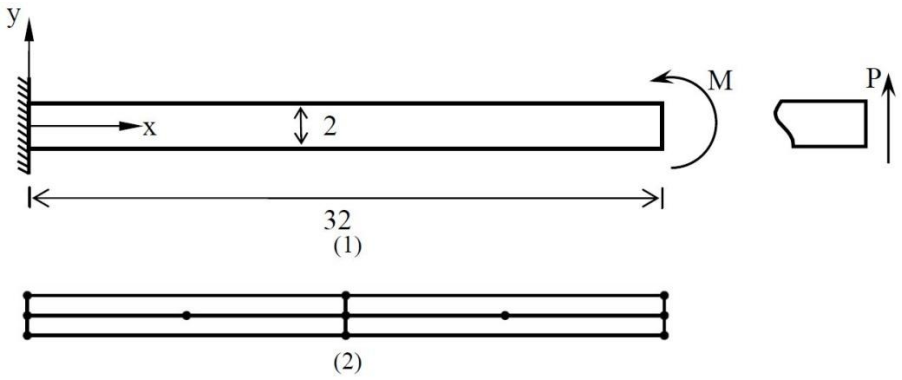

Figure 7.Slender cantilever beam.

The deflection of the homogeneous slender cantilever beam under a shear force at its free end is given in Table 2. The curves representing the response of this structure are shown in Fig. 8. This figure indicates that elements SSDD, SSDI, CTE2, stressRP and BODT rapidly converge to the exact answer and are more efficient than the other elements. The behavior of these elements is quite similar in this problem and their respective error is less than one percent.

For meshes with Ny=1, the free-end deflection of the homogeneous slender beam under bending moment is given in Table 3. For a similar beam with Ny=2, these deflection values are presented in Table 4. The results of using elements proposed by other researchers are also given in these two tables. The curves related to these responses are shown in Figs. 9 and 10. Examining these results indicates that the SSDD and SSDI elements have its superiority for all cases of the meshing. The authors' elements are able to reach exact solution even for coarse meshes with a large aspect ratio. This property clearly demonstrates that the suggested elements are free from parasitic shear error.

Table 2.Free-end deflection of the slender beam under shear loading.

element	$N_x \times N_y$						
	1×1	**2×1**	**4×1**	**8×1**	**16×1**	**32×1**	**64×1**
strainRP	70.35	87.88	92.26	93.35	93.63	93.71	93.73
stressRP	75.02	93.72	98.39	99.56	99.86	99.94	99.97
DispRP	0.97	3.75	13.39	37.49	68.16	85.69	91.58
BODT	75.20	93.37	98.20	99.55	99.93	100.12	100.15
ALL-EX	0.24	0.69	6.36	35.18	59.59	65.70	67.03
CST	0.48	1.14	4.62	12.66	22.88	28.73	30.69
SSDD	75.14	93.78	98.42	99.58	99.86	99.93	99.95
CTE1	47.13	59.54	65.05	73.27	85.84	95.05	98.59
CTE2	74.65	93.25	97.90	99.06	99.35	99.42	99.44
SSDI	75.01	93.71	98.39	99.56	99.85	99.93	99.95

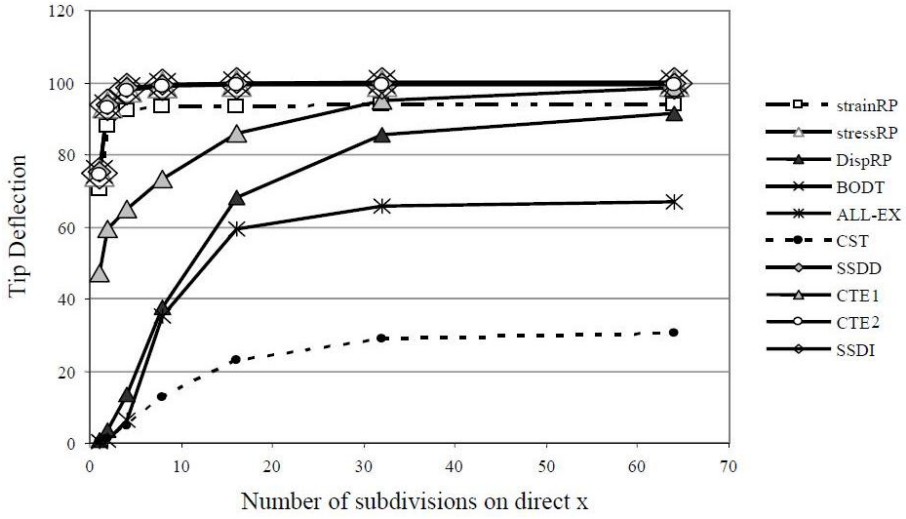

Figure 8.Free-end deflection of the slender beam under shear loading.

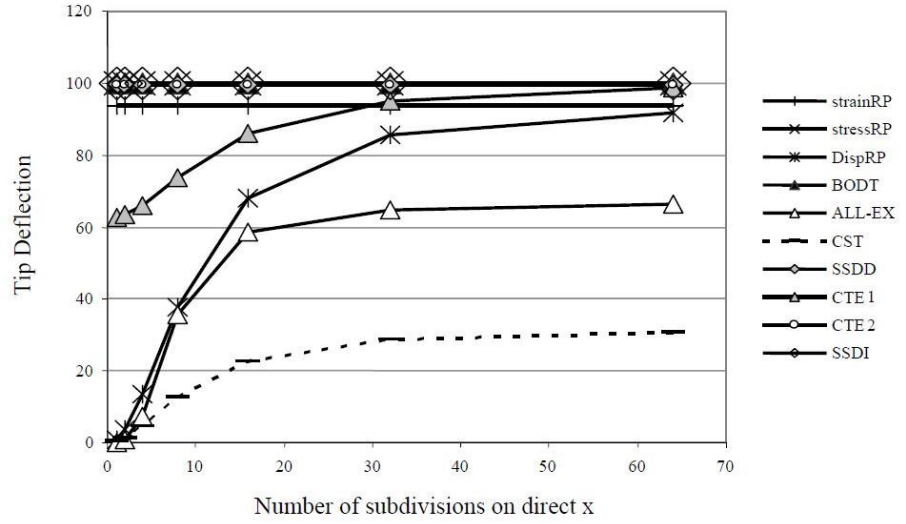

Figure 9.Free-end deflection of the slender beam under bending moment for N_y=1

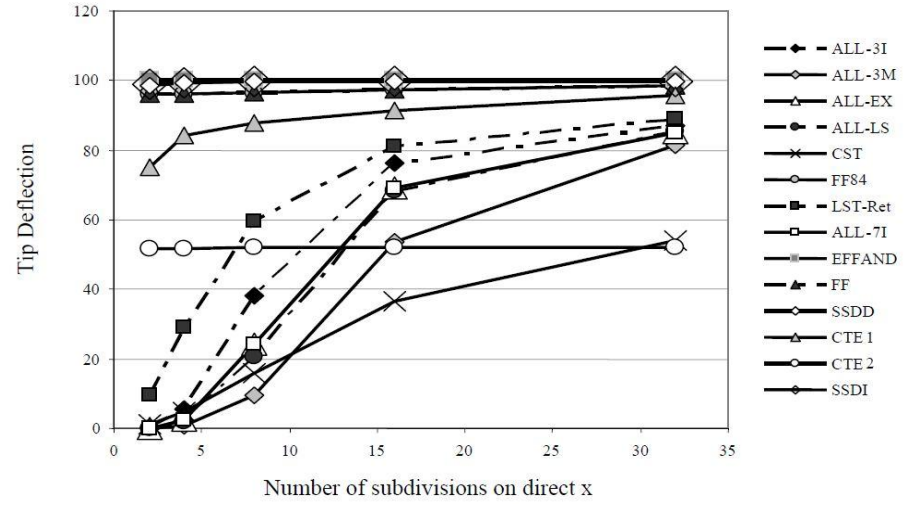

Figure 10.Free-end deflection of the slender beam under bending moment for N_y=2

Table 3.Free-end deflection of the slender beam under bending moment.

element	$N_x \times N_y$						
	1×1	**2×1**	**4×1**	**8×1**	**16×1**	**32×1**	**64×1**
strainRP	93.75	93.75	93.75	93.75	93.75	93.75	93.75
stressRP	100.00	100.00	100.00	100.00	100.00	100.00	100.00
DispRP	0.97	3.75	13.39	37.49	68.18	85.71	91.60
BODT	100.00	100. 00	100. 00	100. 00	100. 00	100. 00	100.00
ALL-EX	0.04	0.63	7.40	35.83	58.44	64.89	66.45
CST	0.32	1.25	4.46	12.50	22.73	28.57	30.53
SSDD	99.84	99.84	99.84	99.84	99.84	99.84	99.84
CTE1	62.74	63.45	66.04	73.53	85.94	95.11	98.64
CTE2	99.48	99.48	99.48	99.48	99.48	99.48	99.48
SSDI	100	100	100	100	100	100	100

Table 4.Deflection of the slender beam under bending moment.

element	$N_x \times N_y$				
	2×2	**4×2**	**8×2**	**16×2**	**32×2**
ALL-3I	0.39	5.42	38.32	76.48	87.08
ALL-3M	0.04	0.71	9.59	53.57	81.36
ALL-EX	0.16	2.47	24.23	69.09	84.90
ALL-LS	0.12	1.89	20.83	68.25	85.36
CST	1.28	4.82	15.75	36.36	54.05
FF84	96.27	96.34	96.58	97.17	98.36
LST-Ret	9.46	28.93	59.58	81.04	89.05
ALL-7i	0.16	2.47	24.25	69.09	84.92
EFF-AND	100.07	99.96	99.99	99.99	99.99
FF	96.27	96.34	96.58	97.17	98.36
SSDD	98.74	99.31	99.62	99.79	99.87
CTE1	75.07	84.17	87.65	91.42	95.94
CTE2	51.56	51.85	52.01	52.10	52.14
SSDI	98.83	99.37	99.68	99.84	99.92

7.3 Cantilever shear wall

In this part, the four elements SSDD, SSDI, CTE1 and CTE2 will be utilized for analyzing a cantilever shear wall. The geometry and loading of this shear wall is illustrated in Fig. 11-1. The elastic modulus and the Poisson's ratio are assumed to be 20000000 kN/m^2 and 0.2, respectively. The loading parameters q and p are respectively set to 500 kN and 100 kN. This shear wall will be analyzed using the different meshes shown in Fig. 11-2. In order to provide a basis for comparison of the robustness and accuracy of the proposed elements, an eight-node element is used to model the structure. The top end lateral drift of the shear wall is evaluated by taking advantage of the suggested and the eight-node isoparametric element with various meshing cases. The OPT1 element will also be used for the comparison. The results of using this element are available for the different meshing cases (Paknahad *et al.*, 2007). These results and the ones obtained from the suggested elements and the eight-node isoparametric element are shown in Fig. 12. It should be mentioned that the OPT1 element is developed for analyzing shear walls. In other words, the OPT1 element is a specialized element for shear wall analysis. The efficiency of the eight-node

isoparametric element is also a well-known fact. Fig.12 demonstrates the advantage of the SSDD and SSDI elements over the OPT1 element, whereby the five-node SSDD and SSDI elements and the strong eight-node isoparametric element yield the similar results.

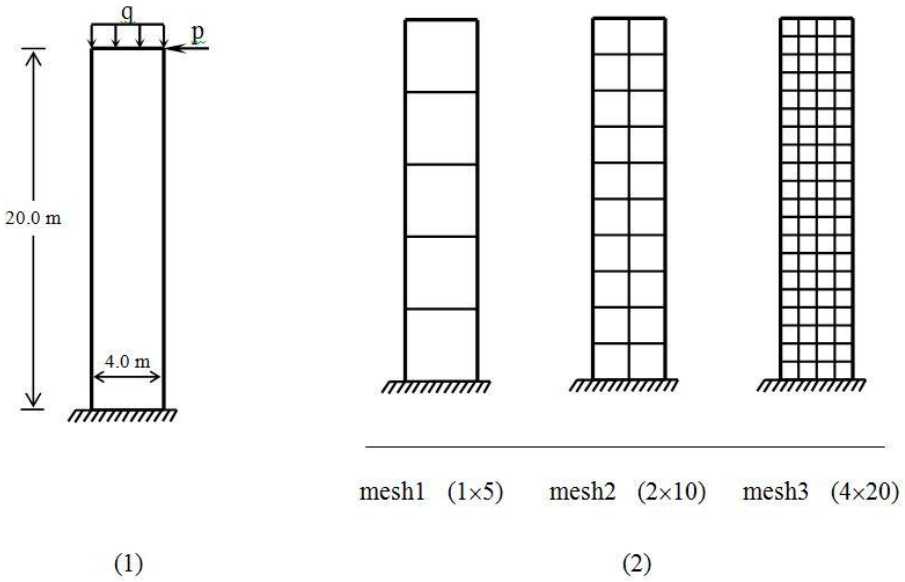

Figure 11.The Geometry, loading and meshing cases of the cantilever shear wall.

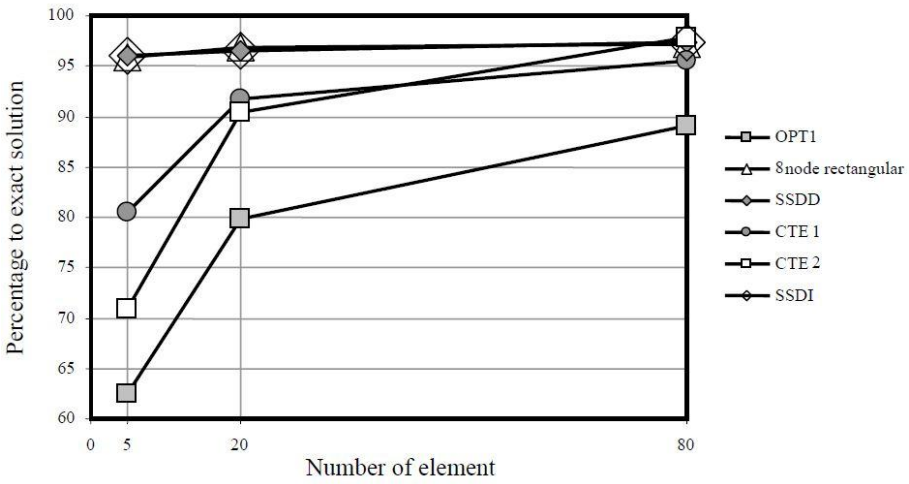

Figure 12.Lateral drift for the top end of the Cantilever shear wall.

7.4 Coupled shear wall

Elements SSDD, SSDI, CTE1 and CTE2 will be used in this section to analyze a coupled shear wall. The geometry and the loading state of this structure are illustrated in Fig. 13-1. The elastic modulus and the Poisson's ratio are respectively equal to 20000000 kN/m2 and 0.25. The width of the wall is 0.4 m and the magnitude of P is equal to 500 kN. The analysis of this shear wall is carried out for two different meshes, cases of a and b. These meshes are shown in Fig. 13-2. The lateral drift of the 2nd, 4th, 6th and 8th stories is calculated using the proposed elements with the two meshing cases. For comparison reasons, element OPT1 is also utilized, which its results are available for this problem (Cook, 1987). In addition, the eight-

node isoparametric element is also implemented in this analysis. The results of all two proposed elements, CTE1, CTE2, the OPT1 element and the eight-node isoparametric element are given in Table 5. For comparison purpose, a very fine mesh of the eight-node isoparametric element is used to analyze the shear wall. In this fine mesh, the entire shear wall is modeled by using 10×10 cm2 elements. This mesh will include 26880 strong eight-node isoparametric elements, which is denoted by c. The near exact solutions belong to the isoparametric elements refined mesh.

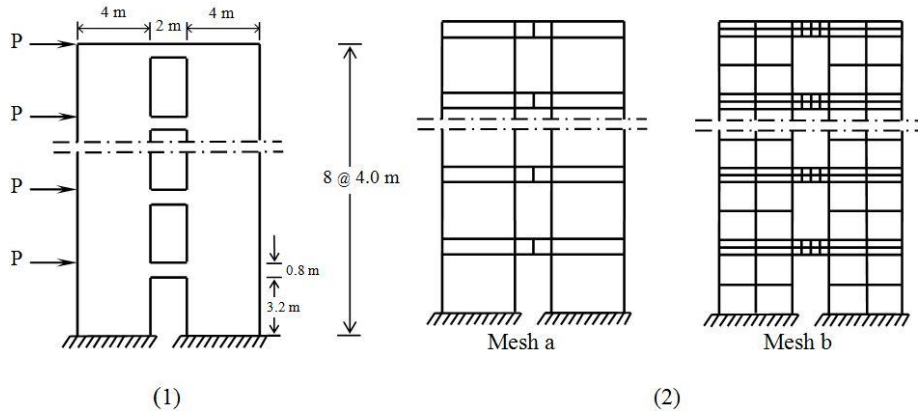

Figure 13.The geometry, loading state and meshing cases for the coupled shear wall.

Table 5 demonstrates the advantage of the proposed elements over the eight-node isoparametric element. For finer meshes, the SSDD element yields better results than OPT1. In comparison to other elements, SSDI leads to best answers for meshes a and b.

Table 5. Lateral displacement of the 2nd, 4th, 6th and 8th stories of the coupled wall.

element	Model	Normalized displacements respect to near exact ones			
		Floor 2	Floor 4	Floor 6	Floor 8
SSDD	*a*	*77*	*79*	*80*	*80*
	b	82	84	85	87
CTE1	*a*	*79*	*80*	*81*	*82*
	b	84	85	86	86
CTE2	*a*	*77*	*79*	*81*	*81*
	b	86	87	89	90
SSDI	*a*	*86*	*87*	*87*	*88*
	b	87	87	88	88
OPT1	*a*	*79*	*80*	*82*	*83*
	b	82	83	84	84
Eight node isoparametric element	*a*	*62*	*64*	*66*	*68*
	b	76	76	77	78
element	**Model**	**Near exact lateral displacement at floor level**			
		Floor 2	**Floor 4**	**Floor 6**	**Floor 8**
Eight node isoparametric element	c	0.9	2.38	3.91	5.35

7.5 Very slender cantilever Subjected to in-plane shear

As it is shown in Fig. 14, the structure has the length of 100, width of 1 and thickness of 1. The elasticity modulus and Poisson's ratio are 10000000 and 0.3, respectively. This beam, which is subjected to a unit force at the tip, is a severe test to evaluate the capability of elements. A 1×100 mesh, which consists of 100 and 1 subdivision in x and y directions, respectively, is solved in this section. The aspect ratio of elements in this mesh equals to one. A 2×100 mesh is also used in this analysis.

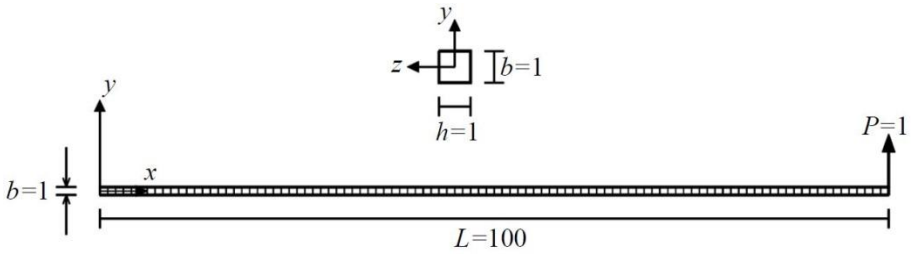

Figure 14. Geometry of slender cantilever subjected to in-plane shear

The exact displacements of the tip in x and y directions are respectively 3 and 4 (Wisniewski and Turska, 2009; Wisniewski *et al.*, 2010). Other results of well-known elements are presented in Table 6. It is noticeable in this table that elements HW12-S and HW10-N have relatively poor accuracy while errors of the suggested elements are small.

Table 6. Displacements of tip of the beam subjected to shear

Elements	Mesh	u_x×100	u_y
HW14-S, HW14-N, HW18	1×100	3	4.0002
	2×100	2.9988	3.9978
HW12-S, HW10-N	1×100	2.73	3.6402
	2×100	2.9264	3.9013
EADG4, HR5-S	1×100	3	4.0002
	2×100	2.9988	3.9978
SSDD	1×100	3.000000	4.000161
	2×100	2.998723	3.997608
CTE1	1×100	2.632500	3.510172
	2×100	2.780537	3.706858
CTE2	1×100	2.730000	3.640169
	2×100	2.926386	3.901192
SSDI	1×100	3.004621	4.006691
	2×100	2.999078	3.998181
(Wisniewski and Turska, 2009)		3	4

8 Conclusions

This paper only discussed the rectangular element, and thus it is especially suited to mesh rectangular shaped domains. In this study, strain gradient notation has been used to develop different optimal criteria for finite elements. Based on these criteria, proper strain states are chosen, and the corresponding displacement field is obtained. Utilizing the equilibrium equations and minimizing the energy functional led to the creation of two five-node models for the plane-strain and plane-stress problems. The presented five-node rectangular elements are insensitive to the aspect ratio and have rotational invariance property. In the proposed formulation, the parasitic shear error can easily be eliminated by excluding the incorrect

strain states from the shear strain polynomial. In the tests of structure having bending deformations, most of the elements in coarse meshes led to the outcomes with large errors. However, the authors' elements can reach near exact solution because the presented elements are free of parasitic shear error. Moreover, solution of the short beam subjected to shear force demonstrated that the proposed strategy is free of shear-locking, as well.

Good accuracy and rapid convergence to the exact solution are other merits of the suggested element. Different benchmark problems were analyzed to confirm the efficiency and the accuracy of the two proposed elements. In this investigation, the authors' elements and those from other researchers were compared. The findings of the paper confirmed that the SSDD and SSDI were the most advantageous elements in solving the plane problems. In all the numerical examples, these elements demonstrated satisfying features such as; insensitivity to the aspect ratio, small error in coarse meshes and rapid convergence to the exact solution. The tests in sections 7-1 and 7-2 verified that in the meshes with a large aspect ratio, having bending and shear deformations, the proposed elements lead to low error responses.

It is worth emphasizing that proper selection of displacement field was led to two elements, which are free of the parasitic shear error. Furthermore, the two other traditional elements also proved to be effective.

References

Allman, D.J. (1984). Compatible triangular element including vertex rotations for plane elasticity analysis. *Computers and Structures*, 19, 1-8.

Allman, D.J. (1988). Evaluation of the constant strain triangle with drilling rotations. *International Journal for Numerical Methods in Engineering*, 26, 2645-2655.

Alvin, K., Fuente, H.M.d.l., Haugen, B.&Felippa, C.A. (1992). Membrane triangles with corner drilling freedoms. I. The eff element. *Finite Elements in Analysis and Design*, 12, 163-187.

Bergan, P.G.&Felippa, C.A. (1985). A triangular membrane element with rotational degrees of freedom. *Computer Methods in Applied Mechanics and Engineering*, 50, 25-69.

Bergan, P.G.&Nygard, M.K. (1984). Finite elements with increased freedom in choosing shape functions. *International Journal for Numerical Methods in Engineering,*, 20, 643-663.

Cook, R.D. (1987). Plane hybrid element with rotational d.O.F. And adjustable stiffness. *International Journal for Numerical Methods in Engineering*, 24, 1499-1508.

Dow, J.O. (1999). A unified approach to the finite element method and error analysis procedures. *Academic Press*.

Dow, J.O.&Byrd, D.E. (1988). The identification and elimination of artificial stiffening errors in finite elements. *International Journal for Numerical Methods in Engineering*, 26, 743-762.

Eom, J., Ko, J.&ChaiLee, B. (2009). A macro plane triangle element from the individual element test. *Finite Elements in Analysis and Design*, 45, 422-430.

Felippa, C. (2000). Recent advances in finite element templates. *Computational Mechanics for the Twenty-First Century*, 71-98.

Felippa, C.A. (2003a). A study of optimal membrane triangles with drilling freedoms. *Computer Methods in Applied Mechanics and Engineering*, 192, 2125-2168.

Felippa, C.A. (2003b). A template tutorial, In *Centro Internacional de Metodos Numericos en Ingeneria (CIMNE)*, Barcelona, Spain.

Felippa, C.A. (2006). Supernatural quad4: A template formulation. *Computer Methods in Applied Mechanics and Engineering*, 195, 5316-5342.

Felippa, C.A.&Alexander, S. (1992). Membrane triangles with corner drilling freedoms: Iii. Implementation and performance evaluation. *Finite Elements in Analysis and Design*, 12, 203-239.

Felippa, C.A.&Militello, C. (1990). Variational formulation of high performance finite elements:Parametrized variational principles. *Computers and Structures*, 36, 1-11.

Felippa, C.A.&Militello, C. (1992). Membrane triangles with corner drilling freedoms: Ii. The andes element. Finite Elements in Analysis and Design(12), 189-201.

Felippa, C.A.&Militello, C. (1999). Construction of optimal 3-node plate bending elements by templates. *Computational Mechanics for the Twenty-First Century*, 24, 1-13.

Ghali, A.&Chieslar, J. (1986). Hybrid finite elements. *Journal of Structural Engineering, ASCE*, 112, 2478-2493.

MacNeal, R.H. (1978). Derivation of element stiffness matrices by assumed strain distribution. *Nuclear Engineering and Design*, 70, 3-12.

Paknahad, M., Noorzaei, J., Jaafar, M.S.&Thanoon, W.A. (2007). Analysis of shear wall structure using optimal membrane triangle element. *Finite Elements in Analysis and Design*, 43, 861-869.

Pian, T.H.H. (1995). State of the art development of hybrid/mixed finite element method. *Finite Element in Analysis and Design*, 21, 5-20.

Wisniewski, K.&Turska, E. (2006). Enhanced allman quadrilateral for finite drilling rotations. *Computer Methods in Applied Mechanics and Engineering*, 195, 6086-6109.

Wisniewski, K.&Turska, E. (2008). Improved four-node hellinger-reissner elements based on skew coordinates. *International Journal for Numerical Methods in Engineering*, 76, 798-836.

Wisniewski, K.&Turska, E. (2009). Improved 4-node hu-washizu elements based on skew coordinates. *Computers and Structures*, 87, 407-424.

Wisniewski, K., Wagner, W., Turska, E.&Gruttmann, F. (2010). Four-node hu-washizu elements based on skew coordinates and contravariant assumed strain. *Computers and Structures*, 88, 1278-1284.

Yeo, S.T.&Lee, B.C. (1996). Equivalence between enhanced assumed strain method and assumed stress hybrid based on the hellinger-reissner principle. *International Journal for Numerical Methods in Engineering*, 39, 3083-3099.